Journal of Microwaves, Optoelectronics and Electromagnetic Applications, Vol. 22, No. 1, March 2023
DOI: http://dx.doi.org/10.1590/2179-10742023v22i1270778

A Multi-Plasmonic Approach for Simultaneous Measurements based on a D-Shaped Photonic Crystal Fiber Sensor: from Temperature to Optical Dispersion

Amanda F. Romeiro[1], Markos P. Cardoso[1], Anderson O. Silva[2], João C. W. A. Costa[1], M. Thereza R. Giraldi[3], José L. Santos[4,5], José M. Baptista[4,6], Ariel Guerreiro[4,5]

[1]*Federal University of Pará, Applied Eletromagnetism Laboratory, Belém Pará, Brazil – romeiro.amanda@gmail.com, markosdenardi@gmail.com, jweyl@ufpa.br.*

[2]*Federal Center for Technological Education Celso Suckow da Fonseca, Rio de Janeiro, Brazil – anderson.osilva@gmail.com*

[3]*Military Institute of Engineering, Rio de Janeiro, Brazil – mtmrocco@gmail.com*

[4]*, INESC TEC, Porto, Portugal, asguerre@fc.up.pt, josantos@fc.up.pt, jmb@staff.uma.pt*

[5]*Faculty of Sciences, University of Porto, Porto, Portugal*

[6]*Faculty of Exact Sciences and Engineering, University of Madeira, Funchal, Portugal*

***Abstract*— The growing demand for multiparameter sensors includes compact devices accompanied by simple calibration processes to distinguish the outputs from each other. This paper evaluates a scheme to determine multiple parameters of a medium using localized surface plasmon resonances (SPR) excited on a D-shaped photonic crystal fiber (PCF) partially covered by two gold layers of different thicknesses. We demonstrate that the proposed sensing platform, once customized to characterize the possible dispersive profiles of the refractive index of the analyte, also allows interrogating the temperature of a sample from a linear relationship. Since the plasmonic resonances are excited at separated and low crosstalk spectral channels, different sensing responses can be obtained simultaneously in the same location of the D-shaped PCF. These features turn out the SPR sensor a suitable tool for simultaneous monitoring of optical dispersion and temperature.**

***Index Terms*—** surface plasmon resonance, Photonic crystal fiber, multiparameter sensing, optical sensors, optical dispersion.

I. INTRODUCTION

Surface plasmon-polaritons (SPPs) are electromagnetic modes that arise from the coupling between light and free electrons at conducting surfaces. Surface plasmons allow to surpass many limits in optical technologies, from near field enhancement to subwavelength optical confinement. Along the

Brazilian Microwave and Optoelectronics Society-SBMO
Brazilian Society of Electromagnetism-SBMag
received 4 Apr 2022; for review 11 Apr 2022; accepted 5 Dec 2022

ISSN 2179-1074

last two decades, the effort into providing feasible techniques to excite and manipulate surface plasmon modes has been crucial to attain a broad variety of innovative technological applications. Nanoscale sized optical waveguides and narrowband filters for communication networks [1]-[2], plasmonic photovoltaic cells [3]-[4], surface-enhanced Raman scattering [5] and surface plasmon resonance (SPR) spectroscopy [6] are some valuable examples. The interaction between local surface plasmon modes excited at adjacent cells of metal-dielectric metamaterials can yield counterintuitive ways to control light propagation [7].

In optical sensing, plasmonic resonances represent a noticeable milestone into achieving quite refined levels of sensitivity and resolution, which are direct results of the large amount of optical power confined at subwavelength scale [8]. The sort of applications includes biochemical sensing, medical diagnosis, monitoring of pipeline integrity in the oil and natural gas industry, among others. Based on the concepts of Krestchmann method to excite SPPs [9], the SPR sensors have evolved from bulky prism configuration to conducting layers fully integrated to optical fibers [10]-[11]. The SPR condition occurs when the guided fiber mode phase matches the phase of the SPP at the interface between the fiber and the conducting layer. Some reported setups comprise the deposition of metallic nanoparticles over the tapered region of an optical fiber [12], grating-based fibers coated by metallic layers [13] or D-shaped fibers covered by conducting slabs on the flat face [14]. Photonic crystal fibers (PCF) are particularly useful to excite plasmonic resonances due to the high mode confinement within a large mode area [15]. SPR sensors based on D-shaped PCFs can be found in several designs [16]-[17].

In previous works, we extensively characterized a SPR sensor composed by a D-shaped PCF coated by gold layers of different thicknesses [18]-[19]. This sensing platform yields multiple SPR channels able to not only detect average constitutive parameters such as refractive indexes but also to accurately describe the optical dispersion of a medium. In this article, we explore further the spectral characteristics of the SPR sensor based on a D-shaped PCF coated by two gold layers aiming at the simultaneous detection of optical dispersion regimes and temperature. Based on numerical results, we discuss how excited plasmonic resonances can offer independent sensing responses suitable for multiparameter readout.

II. The Designed Structure

The perspective view of the proposed sensor is depicted in Fig. 1 (a). The sensing configuration consists of a D-shaped PCF with diameter D = 24 μm composed by a hexagonal arrangement of air holes incrusted in fused silica. The region with absence of air holes has a diameter of 5 μm. The distance between two consecutive air holes (pitch) is Λ = 2 μm and the diameter of each air hole is d = 1.76 μm. This type of fiber can be fabricated from a stack-and-draw process [20] accompanied by a side-polishing or controlled etching technique [21] to obtain the D-shape of the fiber cross-section.

Brazilian Microwave and Optoelectronics Society-SBMO *received 4 Apr 2022; for review 11 Apr 2022; accepted 5 Dec 2022*
Brazilian Society of Electromagnetism-SBMag *ISSN 2179-1074*

Two gold slabs of equal width $W = 4$ μm but with different thickness ($t_1 = 25$ nm and $t_2 = 40$ nm) are deposited on the flat surface of the fiber to achieve two distinct and independent plasmonic resonances. In practice, a CVD (chemical-vapor deposition) process [22] is suitable to design the gold slabs on the top of the D-shaped PCF. A highlighted view of the gold layers is presented in Fig. 1 (b).

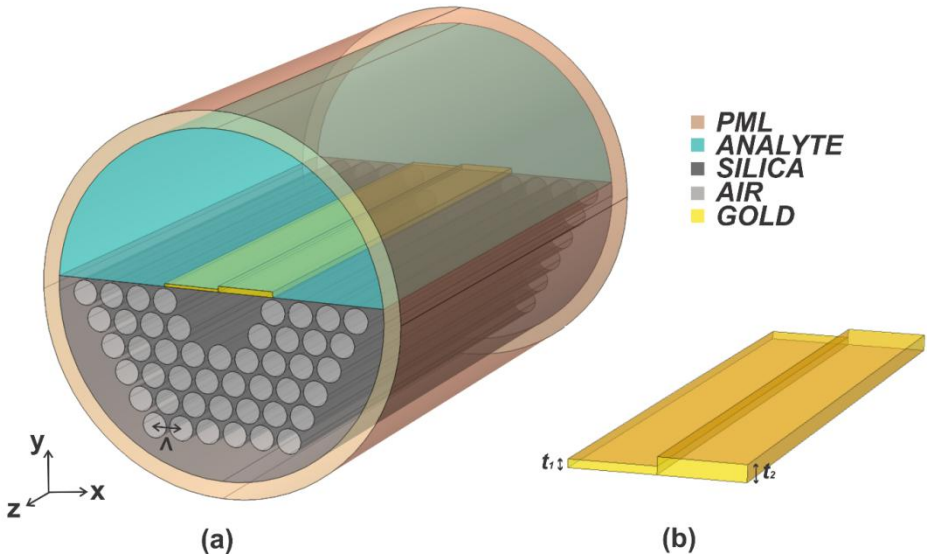

Fig. 1. D-shaped photonic crystal fiber coated by gold slabs sensing platform. (a) Perspective view of the sensor. The entire fiber diameter is $D = 24$ μm, the diameter of each air hole is $d = 1.76$ μm and the pitch is $\Lambda = 2$ μm. The outermost layer that encloses the entire domain corresponds to a 0.1D thick PML. (b) Highlight of the two gold slabs deposited on the top of the flat face of the PCF. They present equal width $W = 4$ μm but different thicknesses: $t_1 = 25$ nm and $t_2 = 40$ nm.

The Finite Element Method based software COMSOL Multiphysics [23] is applied to model numerically the proposed sensor. The computational domain is formed by the fiber cross-section shown in Figure 1(a), truncated by a 0.1D thick PML (Perfectly Matched Layer). The Wave Optics package in the frequency domain is applied to carry out eigenvalue calculations of the Helmholtz equation in the angular frequency ω:

$$\nabla_{\perp}^2 E(r_{\perp}, \omega) + k_0^2(\varepsilon(\omega) - n_{eff}^2) E(r_{\perp}, \omega) = 0 \quad (1)$$

In (1), k_0 is the magnitude of the free-space wavevector and ε is the complex dispersive relative permittivity. $E(r_{\perp},\omega)$ is the modal electric field distribution at the position $r_{\perp}$ perpendicular to the direction of light propagation. The effective index n_{eff} is associated to the resultant mode that arises from the coupling between the fundamental fiber mode and the SPP excited at the conducting interface. The real part of n_{eff} is related to the mode phase and the imaginary part corresponds to the losses of the confined mode due to the penetration of the evanescent fields into the gold layers.

An accurate solution of (1) at the optical domain must regard the dispersive characteristics of all materials involved in the design of the sensor. To model the dispersive character of gold, we applied the corrected Drude-Lorentz formalism [24], an improvement of the original analytical Drude model

ISSN 2179-1074

better adjusted to the corresponding experimental data:

$$\varepsilon_{Au}(\omega) = \varepsilon_{\infty} - \frac{\omega_p^2(T)}{\omega(\omega + i\gamma_t(T))} - \frac{\Delta\epsilon\Omega_L^2}{(\omega^2 - \Omega_L^2) + i\omega\Gamma_L} \tag{2}$$

Where ε_{∞} = 5.9673 stands for the residual polarization of gold at high frequencies and the correction factors are given by $\Delta\epsilon$ = 1.09, Ω_L = 650.07 THz and Γ_L = 104.86 THz.

The influence of the temperature T on (2) is included in the plasma frequency ω_p (T) and in the damping factor γ_t (T) according to the Alabastri model [25]:

$$\omega_p(T) = \omega_p[1 + \gamma_e(T - T_0)]^{-1/2} \tag{3}$$

$$\gamma_t(T) = \gamma_0 + \gamma(T) - \gamma(T_0) \tag{4}$$

In (3) and (4), T_0 is the room temperature and ω_p and γ (T_0) are the corresponding plasma and collision frequencies at T_0, respectively. The constant γ_e=14.2x10^{-6} K^{-1} is the expansion coefficient of gold and γ_0 = 8.04x10^{13} rad/s is the intraband damping coefficient. The γ (T) depends on two factors: phonon–electron scattering and electron–electron scattering. The temperature-dependent collision frequency γ_{ep}(T) is due to phonon-electron scattering and can be obtained from the Holstein model [26]:

$$\gamma_{cp}(T) = \gamma_0\left[\frac{2}{5} + 4\left(\frac{T}{T_D}\right)^5 \int_0^{T_D/T} \frac{z^4 dz}{e^z - 1}\right] \tag{5}$$

Where T_D=170K is the Debye temperature.

The contribution γ_{ce} due to electron-electron scattering can be modeled by using the Lawrence model [26]:

$$\gamma_{ce}(T) = \frac{1}{6}\pi^4 \frac{\Gamma\Delta}{hE_f}\left[(k_B T)^2 + \left(\frac{h\omega}{4\pi^2}\right)^2\right] \tag{6}$$

Where Γ=0.55 is the average scattering probability over the Fermi surface, Δ=0.77 is the fractional Umklapp scattering, E_F = 5.53 eV is the Fermi energy, h is the Plank constant and k_B is the Boltzmanm constant.

The effect of the temperature in the fiber is included in the Sellmeier expression for the refractive index of silica [27].

  ISSN 2179-1074

$$n(\lambda, T) = \sqrt{A + \frac{B}{(1 - C/\lambda^2)} + \frac{D}{(1 - E/\lambda^2)}} \tag{7}$$

Where, A=0.69x10^{-5}T+1.31552, B=2.35835x10^{-5}T+0.788404, C=5.84758x10^{-7}T+0.0110199, D=5.48368 x10^{-7}T+0.91316 and E=100.

III. Modelling and Results

The surface plasmon resonance arises from the phase-matching between the fundamental fiber mode and the surface plasmon mode at the gold interface. At this point, field penetration into the gold layers is maximum and a peak in the losses can be observed. Fig. 2 displays the real and imaginary components of the effective index of the fundamental fiber mode and SPP dispersion curves for a sample with refractive index equal to 1.36 and for room temperature. The imaginary part of n_{eff} is depicted in terms of the confinement losses α [28]:

$$\alpha = 8{,}686 \times {}^{2\pi}/_{\lambda} \times Im_{neff} \times 10^4 \left(\frac{dB}{cm}\right), \tag{8}$$

where λ represents the wavelength and Im_{neff} is the imaginary part of the effective mode index.
Although the fundamental mode of the PCF is degenerate for two orthogonal polarizations, only the polarization perpendicular to the gold interfaces can match the phase of the surface plasmon mode [18]-[19]. Considering the orientation axes shown in Fig. 1, only the Y-polarized fundamental fiber mode is therefore capable of contributing to the SPR condition.

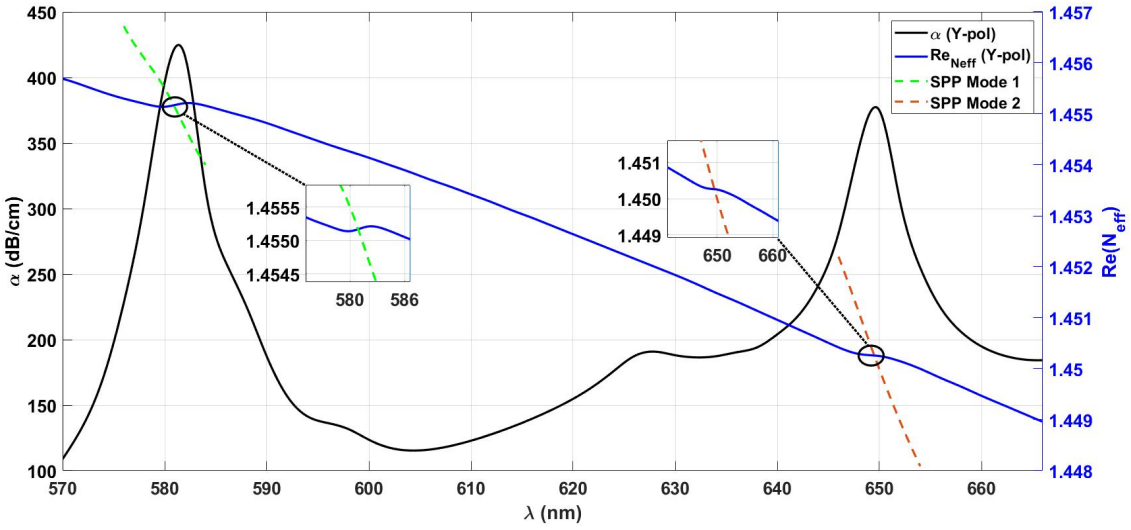

Fig. 2. Effective indexes of the confined modes in the SPR sensor based on a D-shaped PCF with two gold slabs of different thicknesses for an analyte with refractive index of 1.36. N_{eff} is the mode index and Y-pol designate the perpendicular polarization to the gold slabs. SPP mode 1 and SPP mode 2 are the dispersion curves of the plasmonic modes excited at the gold slabs of thicknesses t_1 and t_2, respectively. The insets show a detailed view of the intersections of the dispersion curves for the fundamental Y-polarized fiber mode and the plasmonic modes at the gold interfaces.

Fig. 3. shows the distribution of the electric field intensity at the different wavelengths over the

received 4 Apr 2022; for review 11 Apr 2022; accepted 5 Dec 2022

ISSN 2179-1074

spectral range shown in Fig. 2, including the resonance wavelengths. Such field distributions correspond to the electric field perpendicular to the surface of the metallic slabs and therefore capable of exciting plasmonic resonances. The fundamental aspect is that the coupling between the fundamental fiber mode and the SPP at the gold interface is maximized when the phase-matching is reached. At $\lambda = 582$ nm (Fig. 3(b)), the major of optical power carried by the fiber mode is transferred to the surface plasmon mode at the thinner gold layer. There is another mode coupling at $\lambda = 650$ nm (Fig. 3(e)) that provides an additional SPR at the thicker gold layer. In this case, however, the coupling is not strong as it is seen for 582 nm. This difference in coupling is the reason of the smaller SPR peak amplitude at 650 nm shown in Fig. 2. On the other hand, Fig. 3(a), (c), (d) and (f) taken at off-resonance wavelengths show that both modes are excited separately, preventing a sharp increase in confinement losses at these wavelengths.

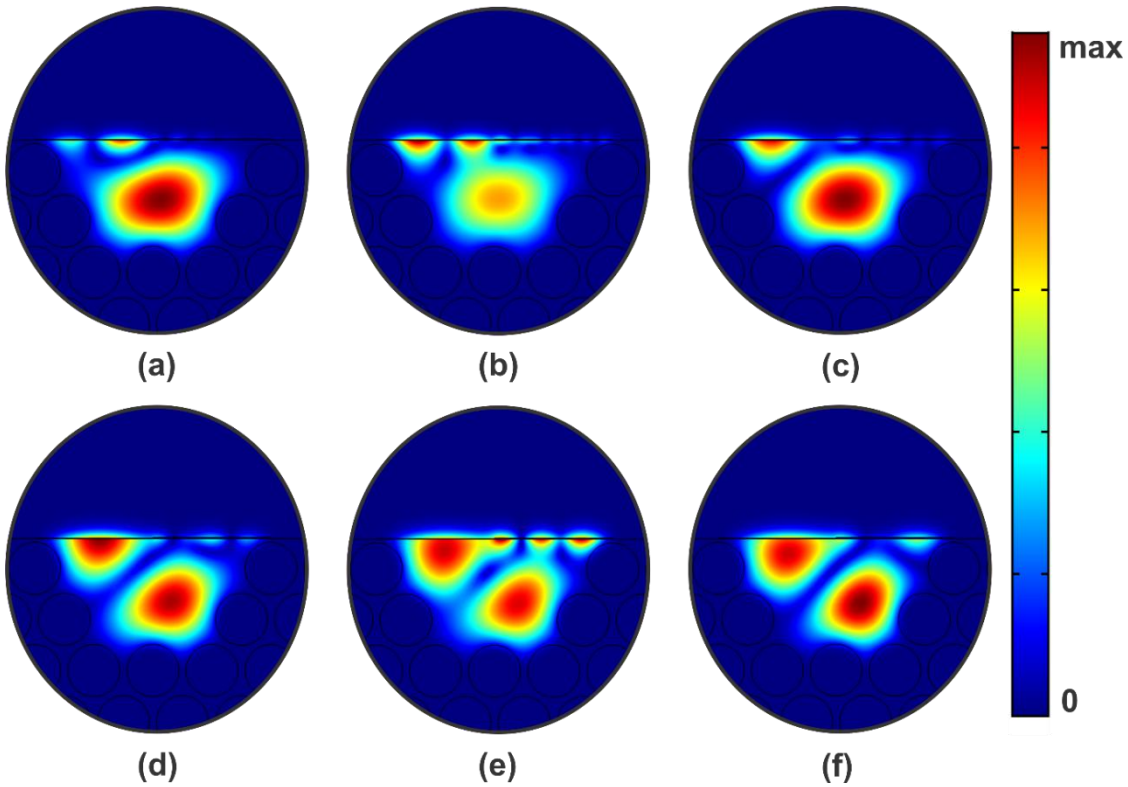

Fig. 3. Distribution of the Y-polarized electric field intensity at the different wavelengths λ: (a) 570 nm, (b) 582 nm, (c) 600 nm, (d) 630 nm, (e) 650 nm and (f) 660 nm.

The wave-coupling restricted by electric fields perpendicular to the conducting interface yields a low crosstalk between SPR spectral channels. As consequence, the SPR sensing platform shown in Fig. 1 can respond unambiguously to the dispersion regime of the external medium. The characterization of the optical dispersion is based on the changes in the spectral distance between the two resonance peaks as illustrated in Fig. 4. (a) Regarding the difference in resonance wavelengths for a constant refractive index as reference, the distance between the two peaks decreases for the anomalous dispersion whereas the normal dispersion leads to a larger difference [18]. Fig. 4. (b)

ISSN 2179-1074

depicts the distance between the wavelength resonance peaks ($\Delta\lambda_{peak}$) for different slopes of the dispersion curves ($dn/d\lambda$). The dots for null dispersion located nearby $\Delta\lambda_{peak} = 68$ nm indicates that the dispersion sensitivity does not depends significantly on the average refractive index. [18].

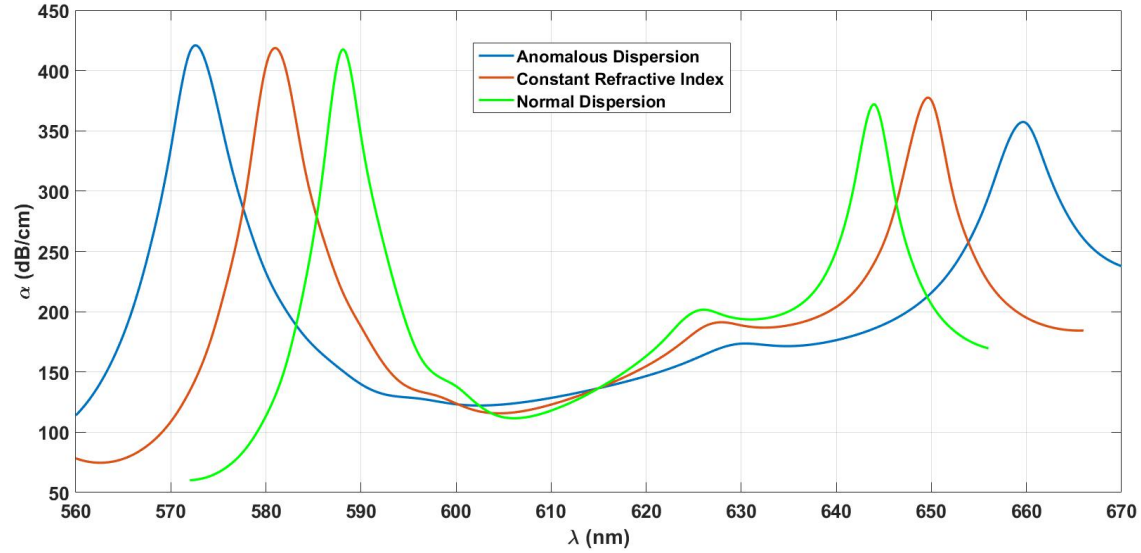

(a)

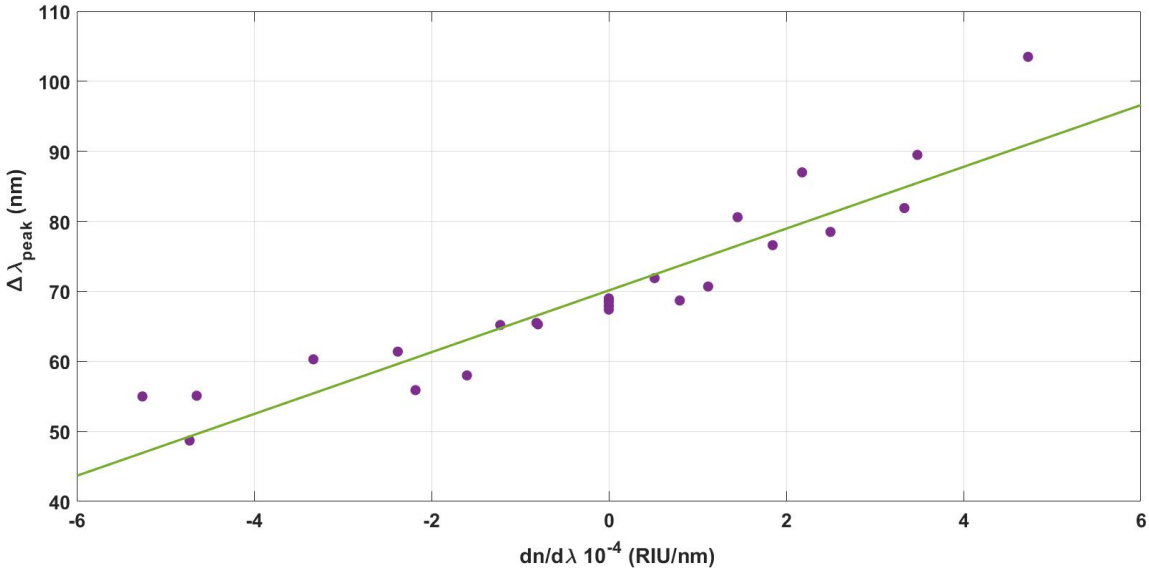

(b)

Fig. 4. (a) Spectral losses of the SPR D-shaped PCF with two gold slabs for different dispersive profiles. (b) Distance $\Delta\lambda_{peak}$ between SPR wavelengths as function of the dispersion slope dn/dλ. The green straight line represents the fitting curve for the computed values.

In the present work, we deal with the perspective of the multichannel SPR sensor being applied to also interrogate temperature.

On the contrary to the sensitivity of the optical dispersion, only the SPR channel excited at the thinner gold layer allows to obtain a linear sensing response to temperature variations. Hence, by considering the first resonance amplitude (which is associated to the SPP mode 1 in Fig. 2) we can estimate the temperature sensitivity of the sensor as:

ISSN 2179-1074

$$S_T = \Delta\alpha_{peak}/\Delta_T \ \text{(dB/cmK)} \tag{9}$$

Where $\Delta\alpha_{peak}$ is the amplitude resonance displacement and Δ_T is defined as the changes in temperature.

Fig. 5 (a) shows the variation in the confinement losses with the temperature for an analyte with refractive index kept fixed at 1.36 for the first peak in Fig. 2. The losses decrease with increasing temperatures at an average sensitivity of -0.86 dB/cmK as displayed in Fig. 5(b).

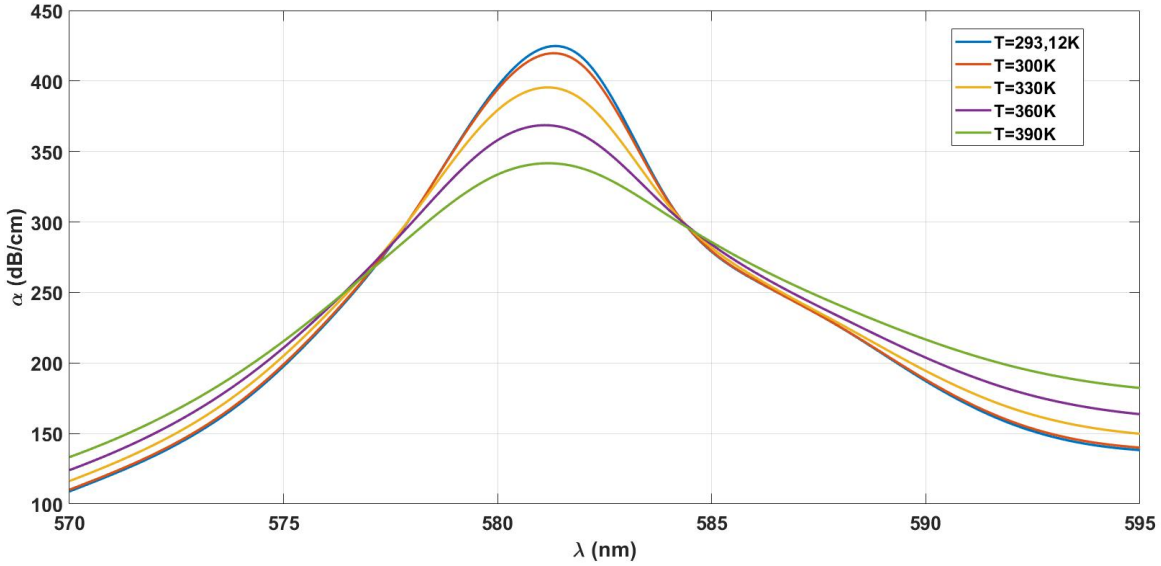

(a)

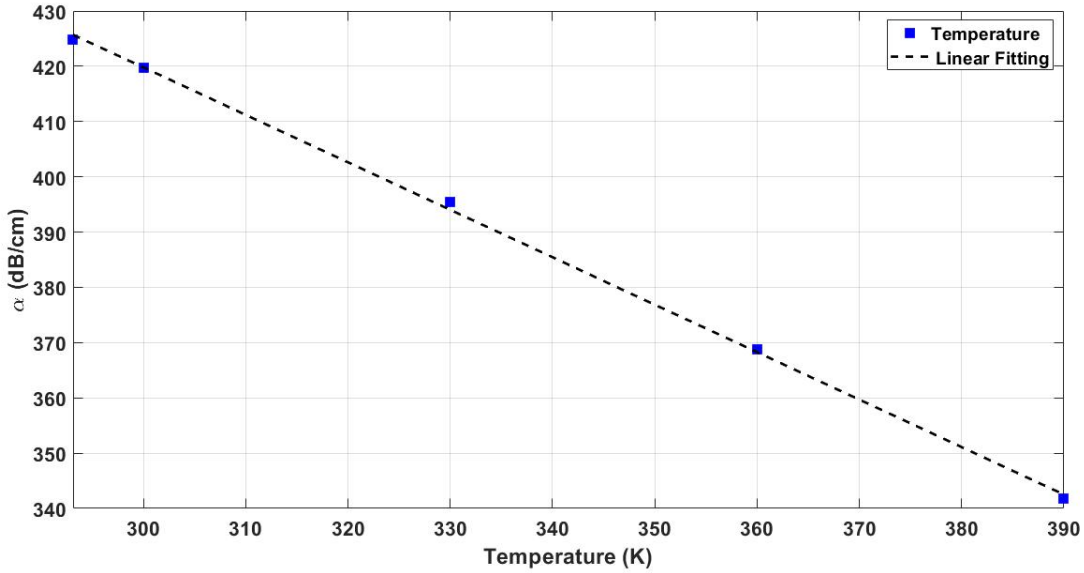

(b)

Fig. 5. (a) Amplitude from the first resonance peak for different temperatures with a refractive index kept fixed at 1.36. (b) Computed data for the amplitude of first peak for different values of temperature and a linear fitting.

received 4 Apr 2022; for review 11 Apr 2022; accepted 5 Dec 2022

ISSN 2179-1074

Since the variations in the temperature are estimated from the amplitude of the SPR peak excited at the thinner gold slab whereas the characterization of the dispersion regime is taken from the distance between resonance wavelengths, we infer that the proposed SPR sensor enables to monitor simultaneously dispersion and temperature. Moreover, the sensing response is obtained at one location of the sensor structure. This is a very attractive feature that reduces the complexity in interrogating several outputs provided by multiparameter optical sensors [29-32]. By allowing simultaneous measurements of multiple quantities at the same place of the fiber, rather than placing specialized sensors sequentially along the fiber, this approach extends the notion of distributed sensing. Indeed, instead of having each quantity measured at a specific location, it is possible to obtain the set of variations of different monitored quantities at separated places of the fiber by distributing several multiple parameter sensors along it.

We can even consider adding the interrogation of refractive indexes to the multichannel SPR sensor. The shifts in the resonance wavelength at the SPR peak excited at the thicker gold slab can be linearly related to changes in the refractive index of the analyte. Nonetheless, we remark that the entire SPR sensing structure is optimized to characterize the dispersive profile of the analyte and thus only a small average sensitivity of 375 nm/RIU for the two SPR spectra can be achieved for refractive indexes in the range [1.3,1.39].

IV. CONCLUSIONS

This paper addressed the potential of a multichannel SPR sensor based on a D-shaped PCF to be applied as a multiparameter sensing platform. The flat surface of the D-shaped PCF is coated by two gold layers of different thicknesses that enable the excitation of two SPR spectral channels based on the waveguide coupling technique. It has already been demonstrated that these two channels present low crosstalk and are sensitive to both normal and anomalous dispersion regimes when analyzed in combination. This work introduced an additional sensing functionality by which the temperature of the analyte is linearly related to the variations in amplitude of the sharper SPR peak. In particular, the proposed SPR sensor comprises two distinct sensing principles that can be applied for a simultaneous measurement of temperature and optical dispersion. These sensing properties are quite appropriate for a better characterization of complex composites as fluidic media with time-varying constituents. Upon a general framework, we summarize that the applicability of the SPR sensor configuration for multiparameter sensing purpose benefits from two independent responses taken at a single location on a D-shaped PCF.

ACKNOWLEDGMENT

This study was financed in part by the Coordenação de Aperfeiçoamento de Pessoal de Nível Superior – Brazil (CAPES) – Finance code 001. During the period of elaboration of this work, the authors have

  ISSN 2179-1074

obtained support from the Conselho Nacional de Desenvolvimento Cientifico e Tecnologico (CNPq), Brazil, as well. It was also financed by the ERDF- European Regional Development Fund through the Operational Program for Competitiveness and Internationalization—COMPETE 2020 Program and by National Funds through the Portuguese funding agency, FCT—Fundação para a Ciência e a Tecnologia within project "GreenNanoSensing" POCI-01-0145-FEDER-032257

REFERENCES

[1] J. Tao, X. G. Huang, X. Lin, Q. Zhang, and X. Jin, "A narrow-band subwavelength plasmonic waveguide filter with asymmetrical multiple-teeth-shaped structure", *Opt. Express,* vol. 17, pp. 13989-13994, 2009.

[2] H. Lu, X. Liu, D. Mao, L. Wang, and Y. Gong, "Tunable band-pass plasmonic waveguide filters with nanodisk resonators", *Opt. Express,* vol. 18, pp. 17922-17927, 2010.

[3] H. Atwater, A. Polman, "Plasmonics for improved photovoltaic devices", *Nature Materials*, vol. 9, pp. 205-213, 2010.

[4] F. J. Beck, A. Polman and K. R. Catchpole, "Tunable light trapping for solar cells using localized surface plasmons", *Journal of Applied Physics*, vol. 105, pp. 114310-114310-7, 2009.

[5] B. Duan, J. J. Zhou, Z. Fang, C. X. Wang, X. J. Wang, H. F. Hemond, M. B. Chan-Park, H. W. Duan, "Surface enhanced Raman scattering by graphene-nanosheet-gapped plasmonic nanoparticle arrays for multiplexed DNA detection", *Nanoscale*, vol 7, pp. 12606-12613, 2015.

[6] S. A. Meyer, E. C. Le Ru and P. G. Etchegoin, "Combining Surface Plasmon Resonance (SPR) Spectroscopy with Surface-Enhanced Raman Scattering (SERS)", *Anal. Chemical*, vol. 83, pp. 2337-2344, 2011.

[7] J. Homola, "Surface Plasmon Polariton Based Sensors", 1st ed., *Springer*, 2018, pp. 3 - 44.

[8] W. L. Barnes, "Surface plasmon-polariton length scales: a route to subwavelength optics", *Journal of Optics A: Pure and Applied Physics*, vol. 8, pp. 87-93, 2006.

[9] J. Homola, I. Koudela, S. S. Yee, "Surface plasmon resonance sensors based on diffraction gratings and prims couplers: sensitivity comparison", *Sensors and Actuators B: Chemical*, vol. 54, pp.16-24, 1999.

[10] Y. Yanase, A. Araki, H. Suzuki, T. Tsutsui, T. Kimura, K. Okamoto, T. Nakatani, T. Hiragun, M. Hide, "Development of an optical fiber SPR sensor for living cell activation", *Biosensors and Bioelectronics*, vol. 25, pp. 1244-1247, 2010.

[11] Y. Zhao, Z.-Q. Deng, Q. Wang, "Fiber optic SPR sensor for liquid concentration measurement", *Sensors and Actuators B: Chemical*, vol. 192, pp. 229-233, 2014.

[12] H.-Y. Lin, C.-H. Huang, G. -L. Cheng, N.-K. Chen and H.-C. Chui, "Tapered optical fiber sensor based on localized surface plasmon resonance", *Optics Express*, vol. 20, pp. 21693-21701, 2012.

[13] S. M. Tripathi, A. Kumar, E. Marin, J.-P. Meunier, "Side-Polished Optical Fiber Grating-Based Refractive Index Sensors Utilizing the Pure Surface Plasmon Polariton", *Journal of Lightwave Technology*, vol. 26, pp. 1980-1985, 2008.

[14] D. F. Santos, A. Guerreiro and J. M. Baptista, "SPR Microstructured D-type optical fiber sensor configuration for refractive index measurement", *IEEE Sensors Journal*, vol. 15, pp. 5472-5476, 2015.

[15] Y. Liu, X. Jing, S. Li, S. Zhang, Z. Zhang, Y. Guo, J. Wang and S. Wang, "High sensitivity surface plasmon resonance sensor based on D-shaped photonic crystal fiber with circular layout", *Optical Fiber Technology*, vol. 46, pp. 311-317, 2018.

[16] Junjie Lu, Yan Li, Yanhua Han, Yi Liu, and Jianmin Gao, "D-shaped photonic crystal fiber plasmonic refractive index sensor based on gold grating", *Applied Optics*, vol. 57, pp. 5268-5272, 2018.

[17] G. An, X. Hao, S. Li, X. Yan, and X. Zhang, "D-shaped photonic crystal fiber refractive index sensor based on surface plasmon resonance", *Applied Optics*, vol. 56, pp. 6988-6992, 2017.

[18] M. P. Cardoso, A. O. Silva, A. F. Romeiro, M. T. R. Giraldi, J. C. W .A. Costa, J. L. Santos, J. M. Baptista, A. Guerreiro. "Multi-plasmonic resonance based sensor for the characterization of optical dispersion using a D-shaped photonic crystal fiber", *IEEE Instrumentation & Measurement Magazine*, vol. 24, pp. 63-68, 2021.

[19] Cardoso, M.P.; Silva, A.O.; Romeiro, A.F.; Giraldi, M.T.R.; Costa, J.C.W.A.; Santos, J.L.; Baptista, J.M.; Guerreiro, A. "Second-Order Dispersion Sensor Based on Multi-Plasmonic Surface Resonances in D-Shaped Photonic Crystal Fibers", *Photonics*, vol. 8, pp. 181, 2021.

[20] G. A. Mahdiraji, D. M. Chow, S. Sandoghchi, F. Amirkhan, E. Dermosesian, K. S. Yeo, Z. Kakaei, M. Ghomeishi, S. Y. Poh, S. Y. 262 Gang, F. R. Mahamd Adikan, "Challenges and solutions in fabrication of silica-based photonic crystal fibers: An experimental study", *Fiber and Integrated Optics*, vol. 33, pp. 85-104, 2014,.

[21] Burcu Guleryuz, Caner Durucan, and Mustafa M. Aslan, "Fabrication of D-type fiber optic sensors with a long interaction length and studying effects of critical parameters on sensor response", *Proc. SPIE, Advanced Environmental, Chemical, and Biological Sensing Technologies XI*, pp. 91060J, 2014;

[22] P. J. Sazio, A. Amezcua-Correa, C. E. Finlayson, J. R. Hayes, T. J. Scheidemantel, N. F. Baril, B. R. Jackson, Dong-Jin W., F. Zhang, 296 E. R. Margine, V. Gopalan, V. H. Crespi, J. V. Badding, "Microstructured optical fibers as high-pressure microfluidic reactors", *Science*, vol. 311, pp. 1583-1586, 2006.

[23] Comsol. Available online: www.br.comsol.com (accessed on 16 March 2022).

[24] A. Vial, A.-S. Grimaut, D. Macías, D. Barchiesi and M. L. Chapelle, "Improved analytical fit of gold dispersion: application to the modelling of extinction spectra with a finite-difference time-domain method", *Physical Review B*, vol. 71, pp. 085416(1)- 303 085416(7), 2005,.

  ISSN 2179-1074

[25] A. Alabastri, S. Tuccio, A. Giugni, A. Toma, C. Liberale, G. Das, F. De Angelis, E. Di Fabrizio, and R. P. Zaccaria, "Molding of plasmonic resonances in metallic nanostructures: Dependence of the non-linear electric permittivity on system size and temperature", *Materials (Basel*), vol. 6, pp. 4879–4910, 2013.

[26] D. F. Santos, A. Guerreiro, J. M. Baptista, "Simultaneous plasmonic measurement of refractive index and temperature based on D-type fiber sensor with gold wires", *IEEE Sensors Journal*, vol. 17, 2439-2446, 2017.

[27] T. Srivastava, R. & JhaDas, , "Highly Sensitive Plasmonic Temperature Sensor Based on Photonic Crystal Surface Plasmon Waveguide", *Plasmonics* vol. 8, pp. 515–521, 2013.

[28] M. P. Cardoso, A. O. Silva, A. F. Romeiro, M. T. R. Giraldi, J. C. W. A. Costa, J. L. Santos, J. M. Baptista, A. Guerreiro. "Tunable plasmonic resonance sensor using a metamaterial film in a D-shaped photonic crystal fiber for refractive index measurements", *Applied Sciences - Optical Sensors and Gauges Based on Plasmonic Resonance*, vol. 12 pp. 2153, 2022.

[29] R. A. Perez-Herrera, M. Bravo, D. Leandro, S. Novais, J. Pradas and M. Lopez-Amo, "Multiparameter Sensor Based on a Multi-Interferometric Serial Configuration For Temperature and Strain Measurements", *IEEE Journal of Selected Topics in Quantum Electronics*, vol. 27, pp. 1-4, 2021.

[30] Z. Zhang, J. He, B. Du, F. Zhang, K. Guo, and Y. Wang, "Measurement of high pressure and high temperature using a dual-cavity Fabry–Perot interferometer created in cascade hollow-core fibers", *Optical Letters,* vol. 43, pp. 6009-6012, 2018.

[31] Y. Wei, C. Liu, Y. Zhang, Y. Luo, X. Nie, Z. Liu, Y. Zhang, F. Peng, Z. Zhou, "Multi-channel SPR sensor based on the cascade application of the Single-mode and multimode optical fiber", *Optics Communications*, vol. 390, pp. 82-87, 2017.

[32] A. F. Romeiro, M. P. Cardoso, A. O. Silva, J. C. W. A. Costa, M. T. R. Giraldi, J. L. Santos, J. M. Baptista, A. Guerreiro. "Multiparameter Plasmonic Resonance Sensor using a D -shaped Photonic Crystal Fiber", *International Microwave and Optoelectronics Conference (IMOC)*, 2021, Fortaleza, Brazil.

  ISSN 2179-1074